

## Promising Directions in Chemical Processing of Methane from Coal Industry. Part 4. Long-term Stability Test

E.V. Matus<sup>1,2\*</sup>, O.V. Tailakov<sup>1</sup>, O.B. Sukhova<sup>2</sup>, A.V. Salnikov<sup>1,2</sup>, O.A. Stonkus<sup>2</sup>,  
M.A. Kerzhentsev<sup>1,2</sup>, S.R. Khairulin<sup>1,2</sup>, Z.R. Ismagilov<sup>1,2</sup>

<sup>1</sup>Federal Research Center of Coal and Coal Chemistry, Siberian Branch, RAS, 18, pr. Sovetskiy, Kemerovo, Russia

<sup>2</sup>Boreskov Institute of Catalysis, Siberian Branch, Russian Academy of Sciences, 5,  
pr. Akademika Lavrentieva, Novosibirsk, Russia

### Article info

Received:  
1 August 2024

Received in revised form:  
8 September 2024

Accepted:  
24 October 2024

### Keywords:

Coal mine methane  
Tri-reforming of methane  
Long-term stability test

### Abstract

For the processing of coal mine methane into hydrogen-containing gas, a catalytic process of methane tri-reforming was studied under long-term testing conditions (800 °C, 100 h). The tests were carried out using the actual composition of the methane-containing mixture recovered by mine drainage systems of the Raspadskaya mine (Kuzbass, Russia). Gas chromatographic analysis of coal mine gas showed that it contains the following components with an average concentration, vol.%: CH<sub>4</sub> – 40.18, N<sub>2</sub> – 36.30, H<sub>2</sub>O – 12.90, O<sub>2</sub> – 9.77, CO<sub>2</sub> – 0.88, C<sub>2</sub>H<sub>6</sub> – 0.25 and C<sub>3</sub>H<sub>8</sub> – 0.04. It was found that the average O/C molar ratio was 0.87, so CO<sub>2</sub> addition to the methane-containing mixture was done to maintain the O/C ratio > 1.1 to ensure stable operation (without significant coke formation) during the catalytic process. Long-term catalytic tests have shown high parameters of the methane tri-reforming process, which were stable over the time of operation. At a temperature of 800 °C, after 100 h of process using the Ce<sub>0.2</sub>Ni<sub>0.8</sub>O<sub>1.2</sub>/Al<sub>2</sub>O<sub>3</sub> catalyst, the hydrogen yield was 85% at a methane conversion of 80%. A comparative analysis of the properties of fresh and spent Ce<sub>0.2</sub>Ni<sub>0.8</sub>O<sub>1.2</sub>/Al<sub>2</sub>O<sub>3</sub> catalyst was performed using low-temperature nitrogen adsorption, powder X-ray diffraction, electron microscopy and thermal analysis. It was established that the mesoporous texture of the catalyst was retained, but the dispersion of the active component decreased. The Ce<sub>0.2</sub>Ni<sub>0.8</sub>O<sub>1.2</sub>/Al<sub>2</sub>O<sub>3</sub> catalyst is resistant to thermal sintering and coking, which ensures no deactivation. The use of tri-reforming technology for the utilization of coal mine methane is a step towards “green” coal mining, ensuring sustainable development of society.

## 1. Introduction

Despite climate policies aimed at a low-carbon future, coal continues to occupy an important place in the fuel and energy sector of many countries. Coal-fired electricity generation accounted for about 36% of the total, remaining the world's largest energy source [1]. In 2024, there were 2422 coal-fired power plants operating worldwide [2]. A high share

of electricity generated from coal is typical for such countries as Botswana (96%), Mongolia (85%), India (75%), Kazakhstan (67%) and China (61%) [3].

Coal mining is carried out in about 70 countries. Depending on the depth, density, overburden, and thickness of the coal seam, coal is extracted from underground or open-pit mines. The contributions from underground and surface production are approximately equal [4]. According to the Global Energy Monitor [5], the coal mining industry today employs nearly 2.7 million workers at 3232 active coal mines.

\*Corresponding author.  
E-mail address: matus\_e@mail.ru

Underground mining is recognized as one of the most dangerous professions in the world. The rate of fatal injuries in the coal mining industry depends on the country and varies from year to year. In particular, the fatal work injury rate of approximately 20 deaths per 100000 workers for miners has been reported in the USA [6]. In Russia, the level of fatal injuries in coal mining amounted to 13 per 100000 workers, including 28 per 100000 employees in mines [7]. This is six times higher compared with the country as a whole (3.3 and 4.5 per 100000 workers for USA and Russia respectively). The world's deadliest mining accidents are caused by methane explosions. Most recently, on September 21, 2024, an explosion occurred in a coal mine in Tabas, South Khorasan Province, Iran. The incident killed at least 51 people and injured 20 more [8].

Methane is naturally generated in coal seams by either a microbiological or thermal process that occurred during the coal formation [9,10]. The amount of methane in naturally occurring gas found in coal seams is typically 80–95%. The remaining components are higher hydrocarbons, nitrogen and carbon dioxide. The greater the temperature, pressure, and duration of coal burial, the higher the coal rank and the greater the amount of methane generated [11]. When mining coal, the integrity of coal seams and surrounding strata is disrupted during mining operations, resulting in the release of gas contained in them. In order to improve the safety of mine operation, much attention is paid to the issues of monitoring and forecasting gas emissions in coal mines. The main factors influencing gas release include the geological occurrence conditions of coal seams, the mine design, and its operating conditions [11]. Firstly, it is necessary to take into account the gas content of coal which is expressed in the volume of gas contained per mass of coal substance in situ ( $\text{m}^3/\text{t}$ ). In general, gas content increases with the depth and rank of coal and can reach  $30 \text{ m}^3/\text{t}$  for anthracite [12]. Secondly, the specific emission rate that represents the total volume of methane released from all sources divided by the total amount of coal produced during a referenced period of time should be taken into account. Since the total volume of the gas released is proportional to the rate of strata destruction resulting from mining activities, the amount of gas released during coal mining increases in proportion to the increase in the rate of coal extraction. For example, for coal mines in Kuzbass, the value of specific methane emissions varies in the range from 1.7 to  $74 \text{ m}^3/\text{t}$  [13]. Generally, coal mines with specific emissions of  $10 \text{ m}^3/\text{t}$  and higher

are considered gassy [11]. Thus, it is high-production underground coal mines that develop coal deposits at great depths at high extraction rates and on a large scale that are more likely to encounter the problem of intense methane emissions.

An effective way to solve the gas emission problems and improve safer mining environments is to capture methane from its source before it can enter the mine airways by drainage techniques [11]. The procedure for degassing coal mines is strictly regulated in each country. For example, according to "Instructions for aerological safety of coal mines" of the Russian Federation [14], drainage is mandatory when:

- ventilation work cannot ensure the methane content in the mine atmosphere of operating mine workings in the amount of up to 1%;
- the natural methane content of the seam exceeds  $9 \text{ m}^3/\text{t}$  of dry ash-free mass and ventilation work cannot ensure that the methane content in the outgoing stream of the mine working is less than 1%;
- the concentration of methane in gas pipelines and gas drainage workings exceeds 3.5%.

The drainage is also used in all cases where the extraction and utilization of coal mine methane is economically profitable.

According Global Methane Initiative (GMI), in 2024 there are approximately 500 coal mine methane recovery and utilization projects at coal mines worldwide [15]. The analysis of the International Coal Mine Methane Project List shows that the leading countries in the processing of coal mine methane are China (126), the United States (87), Germany (53), the United Kingdom (38) and Australia (34). Rational ways to process coal mine methane include technologies such as methane destruction in flares; obtaining electrical and thermal energy in modular thermal power plants; combustion of methane-air mixture in boiler units of mine boiler houses; catalytic after burning of methane in gas turbine units; production of chemical products [11]. Among the end-use options for methane, heat and power generation (286) are the first, followed by projects of flaring (83) and gas sales to pipeline (40). There is little work devoted to the use of coal mine methane as a raw material for the synthesis of chemical products and, as a rule, they are carried out at the stage of laboratory research [16–21]. In particular, it has been proposed to use coalbed methane to produce methanol both by direct partial oxidation and from synthesis gas [21]. The optimal conditions for obtaining synthesis gas from coalbed methane for non-catalytic methanol production were evaluated.

In this case, the use mixture with a fuel-air equivalence ratio of at least 4 should be applied. If catalysts are used, synthesis gas can be obtained from leaner mixtures with an equivalence ratio of 3. The use of porous fillers ( $\text{Al}_2\text{O}_3$  and  $\text{ZrO}_2$ ) or a Ni catalyst makes it possible to reduce the conversion temperature of the coal mine methane and obtain hydrogen-containing gas with a concentration of 12 to 45 vol.% of dry gas [16,20].

In our works for the purpose of developing technology for chemical processing of methane from coal industry into valuable products, thermodynamic analysis of the major chemical reactions that occur in the multicomponent system  $\text{CH}_4\text{--CO}_2\text{--H}_2\text{O}$ –air is carried out and optimal conditions of the processes ensuring complete methane conversion and maximal yield of useful products are determined [22], an effective catalyst composition and a method for its synthesis were developed [23], and screening tests were successfully carried out in model mixtures [24]. The question of the activity and resistance of this catalyst to deactivation during processing of the actual composition of coal gas remains open.

Therefore, this work is devoted to studying the features of tri-reforming processing of methane-containing gas recovered by mine drainage systems of the Rospadskaya mine (Kuzbass, Russia) that continues our research on the chemical processing of coal mine gas [22–24].

## 2. Experimental

### 2.1. Catalyst preparation and characterization

$\text{Ce}_{0.2}\text{Ni}_{0.8}\text{O}_{1.2}/\text{Al}_2\text{O}_3$  catalyst was prepared by citrate sol-gel method using  $\text{Al}_2\text{O}_3$  as support and  $\text{Ce}(\text{NO}_3)_3 \cdot 6\text{H}_2\text{O}$ ,  $\text{Ni}(\text{NO}_3)_2 \cdot 6\text{H}_2\text{O}$  and  $\text{C}_6\text{H}_8\text{O}_7$  as initial reagents [25]. The molar ratio of citric acid/(Ce + Ni) was 0.25, the Ni content was ~10 wt.%, Ce – ~6 wt.%. The  $\text{Al}_2\text{O}_3$  support was previously calcined at 850 °C for 6 hours. The thermal treatment of the catalyst included drying at 90 °C and following calcination at 500 °C for 4 hours.

Samples before and after catalytic tests were studied using a set of methods: low-temperature nitrogen adsorption on a Quadrasorb evo unit (Quantachrome Instruments, USA), X-ray phase analysis (XRD) on an ARL X'tra diffractometer (Thermo Fisher Scientific, USA) using  $\text{CuK}\alpha$  radiation (wavelength 1.5418 Å), transmission electron microscopy (TEM) on JEM-2200FS (JEOL Ltd., Japan) and Themis Z (Thermo Fisher Scientific, USA) electron microscopes, simultaneous thermal analysis (thermogravimetric

analysis (TGA), differential thermogravimetric analysis (DTGA), differential thermal analysis (DTA)) using an STA 449 C Jupiter device (NETZSCH-Geratebau GmbH, Germany) [26].

### 2.2. Coal mine gas characterization

The qualitative and quantitative composition of the methane-air mixture recovered by mine drainage systems of the Rospadskaya mine (Kuzbass, Russia) was determined by gas chromatography on a Kristall 5000.2 chromatograph.

### 2.3. Catalyst testing

The catalyst testing was carried out in a flow quartz reactor (internal diameter 11 mm) at atmospheric pressure, contact time 0.15 s, flow rate 200 ml/min. For the catalytic activity testing, a 500 mg sample with a grain size of 250–500  $\mu\text{m}$  was used. Initially, the catalyst was treated in situ at 800 °C for 1 h in  $\text{H}_2\text{+He}$  (screening test) or He (stability test) flow.

The screening test was performed in the stepwise temperature rise mode 650→850 °C. The heating rate was 10 degrees per minute; the holding time at each temperature was 40 minutes. The stability test was performed for 100 h at 800 °C.

The composition of the reaction mixture was analyzed by gas chromatography on a Kristall 2000M chromatograph. The separation of  $\text{H}_2$ , He, CO,  $\text{CO}_2$ ,  $\text{CH}_4$ ,  $\text{C}_2\text{H}_6$  and  $\text{C}_3\text{H}_8$  was carried out on a steel-packed column 2 m long, 3 mm in diameter with SKT carbon (thermal conductivity detector, carrier gas – Ar, flow – 30 ml/min, temperature 130 °C). The following reaction indicators were calculated:

$$\text{CH}_4 \text{ conversion, \%: } X_{\text{CH}_4} = 100 \times \frac{(F_{\text{CH}_4}^{\text{in}} - F_{\text{CH}_4}^{\text{out}})}{F_{\text{CH}_4}^{\text{in}}},$$

$$\text{CO}_2 \text{ conversion, \%: } X_{\text{CO}_2} = 100 \times \frac{(F_{\text{CO}_2}^{\text{in}} - F_{\text{CO}_2}^{\text{out}})}{F_{\text{CO}_2}^{\text{in}}},$$

$$\text{H}_2 \text{ yield, \%: } Y_{\text{H}_2} = 100 \times \frac{F_{\text{H}_2}^{\text{out}}}{(2F_{\text{CH}_4}^{\text{in}} + F_{\text{H}_2\text{O}}^{\text{in}} + 3F_{\text{C}_2\text{H}_6}^{\text{in}} + 4F_{\text{C}_3\text{H}_8}^{\text{in}})},$$

$$\text{CO yield, \%: } Y_{\text{CO}} = 100 \times \frac{F_{\text{CO}}^{\text{out}}}{(F_{\text{CH}_4}^{\text{in}} + F_{\text{CO}_2}^{\text{in}} + 2F_{\text{C}_2\text{H}_6}^{\text{in}} + 3F_{\text{C}_3\text{H}_8}^{\text{in}})},$$

where  $F_i$  is the molar flow rate of reagent (i) at the inlet (in) and outlet (out) of the reactor.

### 3. Results and discussion

#### 3.1. Characterization of coal mine gas and its catalytic conversion

Sampling was carried out and the composition of the methane-air mixture recovered by mine drainage systems of the Rospadskaya mine was analyzed. The selection of this mine among the coal mines of Kuzbass was made based on cluster analysis [13]. The Rospadskaya mine is characterized by high values of specific ( $\sim 50 \text{ m}^3/\text{t}$ ) and absolute ( $\sim 350 \text{ m}^3/\text{min}$ ) methane emissions. Table 1 presents the average gas composition, as well as the minimum and maximum values of component concentrations. The composition of the methane-air mixture changed from day to day and varies within the following limits, vol.%: methane – 27–64, oxygen 6–13, nitrogen 20–50, water vapor 6–19, carbon dioxide 0–2, ethane – 0–0.5, propane – 0–0.5. The O/C molar ratio ranges from 0.32 to 1.50, with an average value of 0.87. When the O/C molar ratio  $< 1.1$ , the addition of an oxygen-containing agent ( $\text{CO}_2$  and/or water) is necessary to ensure a stable regime (without significant coke formation) of the tri-reforming process of coal mine methane with a high yield of target products [27]. The composition of the methane-air mixture, taking into account pretreatment, which consists of the addition of an oxygen-containing agent for mixtures with a molar ratio O/C  $< 1.1$ , is indicated in Table 1. It was revealed that a one-component additive (carbon dioxide) is sufficient for optimization of the O/C molar ratio.

Figure 1 demonstrates the temperature dependence of the concentration of reagents, conversion of methane and carbon dioxide, yield of hydrogen and carbon monoxide in tri-reforming of the methane-air mixture recovered by mine drainage systems of the Rospadskaya mine. As the reaction temperature increases from 600 to 850 °C, a de-

crease in the concentration of the initial reagents and an increase in the concentration of the reaction products in the mixture are observed. In particular, the concentration of methane decreases from 18 to 2 vol.%, and hydrogen increases from 24 to 42 vol.%. Already at 600 °C, a fairly high methane conversion occurs – 40%. Considering the absence of carbon dioxide conversion in this temperature range, the main oxygen-containing reagents in the low-temperature range are oxygen and water. Noticeable  $\text{CO}_2$  conversion begins at 700 °C. All reaction parameters (conversion – X and product yield – Y) improve with increasing reaction temperature, reaching the highest values at 850 °C:  $X(\text{CH}_4) = 93\%$ ,  $X(\text{CO}_2) = 82\%$ ,  $Y(\text{H}_2) = 90\%$  and  $Y(\text{CO}) = 95\%$ . Note that these values are close to those achieved under thermodynamic equilibrium conditions at the same temperature:  $X(\text{CH}_4) = 99\%$ ,  $X(\text{CO}_2) = 84\%$ ,  $Y(\text{H}_2) = 94\%$  and  $Y(\text{CO}) = 95\%$  (Fig. 2). At low temperatures, the reaction parameters are lower than thermodynamically possible due to kinetic limitations.

Long-term testing showed the stability of reaction parameters over time (Fig. 3). In the initial period, conversion and yield values increase slightly, and then practically reach a plateau. As noted in the experimental part, before the long-term experiment, the catalyst was not reduced, but was treated in He. Therefore, the formation of particles of catalytically active metallic  $\text{Ni}^0$  occurred *in situ* under the reaction conditions. Consequently, at the initial stage of the reaction, the number of active  $\text{Ni}^0$  sites increased, which led to an increase in the reaction performance. At a temperature of 800 °C after 100 h of process, the hydrogen yield was 85% at a methane conversion of 80%. Note that the ability of the catalyst to be activated by the reaction medium is advantageous because it allows it to operate effectively in a daily startup–shutdown (DSS) regime without additional treatment.

**Table 1.** The composition of the methane-air mixture recovered by mine drainage systems of the Rospadskaya mine

| Specification of mixtures according to component content | Component composition of gas, vol.% |              |                      |               |              |                        |                        |
|--|-------------------------------------|--------------|----------------------|---------------|--------------|------------------------|------------------------|
|  | $\text{CH}_4$                       | $\text{O}_2$ | $\text{H}_2\text{O}$ | $\text{CO}_2$ | $\text{N}_2$ | $\text{C}_2\text{H}_6$ | $\text{C}_3\text{H}_8$ |
| Initial mixture  |                                     |              |                      |               |              |                        |                        |
| Average  | 40.18                               | 9.77         | 12.90                | 0.88          | 36.30        | 0.25                   | 0.04                   |
| Minimum  | 27.10                               | 5.50         | 6.38                 | 0.40          | 20.40        | 0.00                   | 0.00                   |
| Maximum  | 64.40                               | 13.40        | 18.60                | 1.91          | 49.80        | 0.53                   | 0.49                   |
| Mixture after $\text{CO}_2$ addition                     |                                     |              |                      |               |              |                        |                        |
| Average  | 35.41                               | 8.61         | 11.37                | 12.65         | 31.99        | 0.22                   | 0.035                  |

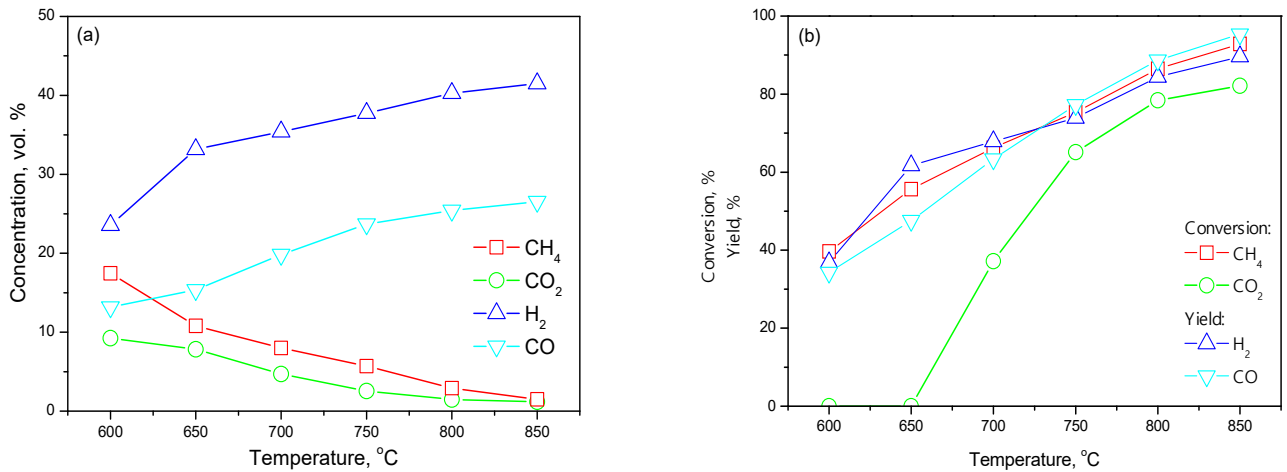


**Fig. 1.** Temperature dependence of concentration of reagents (a), conversion of methane and carbon dioxide (b), yield of hydrogen and carbon monoxide (b) in tri-reforming of the methane-air mixture recovered by mine drainage systems of the Raspadskaya mine

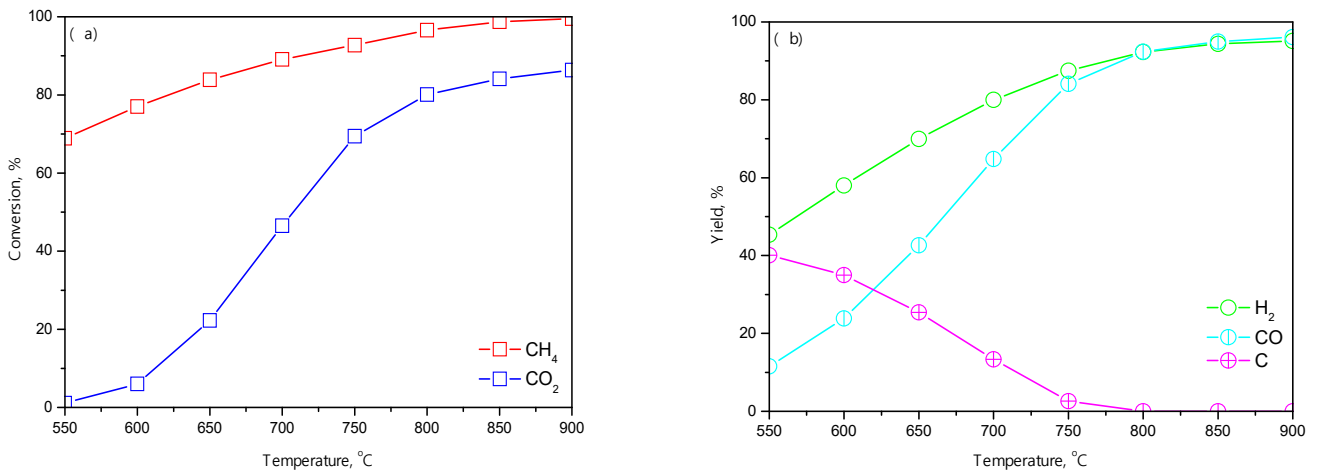


**Fig. 2.** Parameters of the tri-reforming process of the methane-air mixture recovered by mine drainage systems of the Raspadskaya mine under conditions of thermodynamic equilibrium.

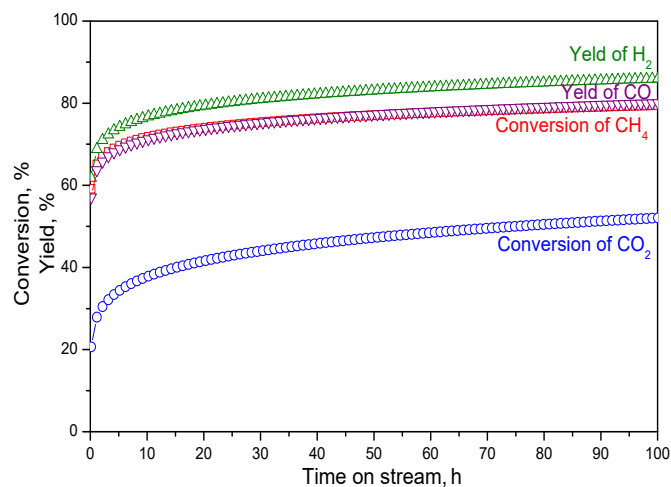


**Fig. 3.** Stability test of the tri-reforming process of the methane-air mixture recovered by mine drainage systems of the Raspadskaya mine. The reaction temperature is equal to 800 °C.

### 3.2. Catalyst resistance to sintering and coking

When using a catalyst in reforming processes, an important issue is its resistance to sintering and coking. So, a comparative analysis of the properties of  $\text{Ce}_{0.2}\text{Ni}_{0.8}\text{O}_{1.2}/\text{Al}_2\text{O}_3$  catalyst before and after the stability test was performed using low-temperature nitrogen adsorption, powder X-ray diffraction, electron microscopy and thermal analysis (Table 2, Fig. 4–6). As was shown earlier [25], the fresh  $\text{Ce}_{0.2}\text{Ni}_{0.8}\text{O}_{1.2}/\text{Al}_2\text{O}_3$  catalyst (after calcination at 500 °C) is a mesoporous material with a specific surface area of 89  $\text{m}^2/\text{g}$  and total pore volume of 0.32  $\text{cm}^3/\text{g}$ . The sample before reaction (after treatment *in situ* in He at 800 °C) retains its textural characteristics

(Table 2) and a mesoporous structure, as evidenced by the obtained adsorption isotherms of type IVa with a hysteresis loop of type H2 (Fig. 4a) according to the IUPAC nomenclature [28]. After the stability test, while maintaining mesoporosity, a moderate decrease in the specific surface area (by ~ 24%) and an increase in the average pore diameter (by ~ 17%) are observed. This may indicate partial blockage of the smallest pores of the material as a result of intensification of sintering processes due to prolonged exposure of the material at a temperature of 800 °C to the components of the reaction medium, especially water vapor. In addition, if carbonaceous deposits are formed during the reaction, they can contribute to changes in textural properties.

**Table 2.** Textural and structural properties of  $\text{Ce}_{0.2}\text{Ni}_{0.8}\text{O}_{1.2}/\text{Al}_2\text{O}_3$  catalysts before and after the stability test in methane tri-reforming reaction

| Sample   | Textural properties      |                           |       | Structural properties   |                              |                                |
|--|--------------------------|---------------------------|-------|---|------------------------------|--------------------------------|
|  | S, $\text{m}^2/\text{g}$ | V, $\text{cm}^3/\text{g}$ | D, nm | Phase composition   | Unit cell parameter, Å       | Coherent scattering region, nm |
| Fresh  | 89                       | 0.32                      | 14.2  | ( $\gamma+\delta$ )- $\text{Al}_2\text{O}_3$<br>CeO <sub>2</sub><br>NiO       | 7.914<br>–<br>–              | –<br>–<br>–                    |
| Before reaction (after treatment <i>in situ</i> in He at 800 °C) | 84                       | 0.34                      | 16.3  | ( $\gamma+\delta$ )- $\text{Al}_2\text{O}_3$<br>CeO <sub>2</sub>              | 7.947<br>5.387               | –<br>4                         |
| After reaction (100 h on stream at 800 °C)                       | 64                       | 0.32                      | 19.1  | ( $\gamma+\delta$ )- $\text{Al}_2\text{O}_3$<br>CeO <sub>2</sub><br>NiO<br>Ni | 7.907<br>–<br>4.179<br>3.529 | –<br>4<br>20<br>17             |

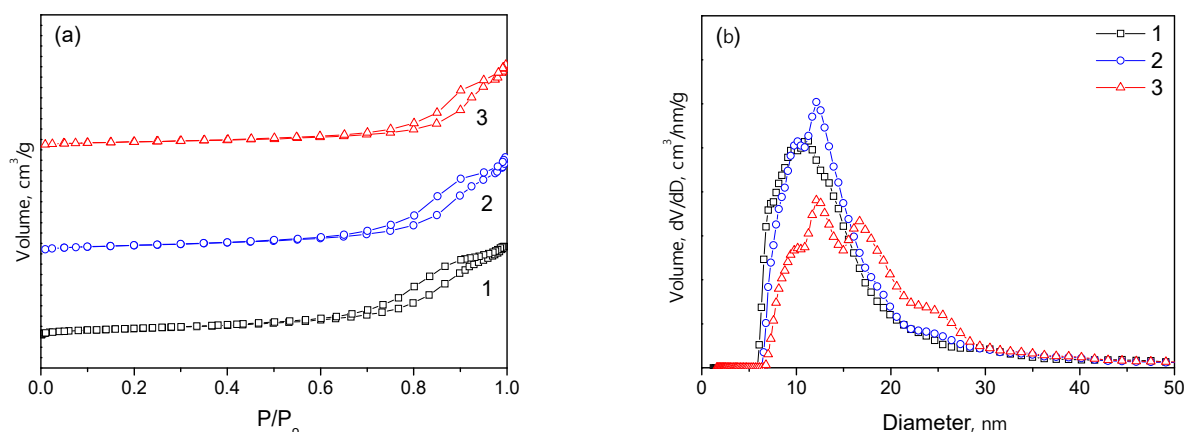


**Fig. 4.** Adsorption isotherms (a) and pore size distribution (b) of fresh  $\text{Ce}_{0.2}\text{Ni}_{0.8}\text{O}_{1.2}/\text{Al}_2\text{O}_3$  catalyst (1), before (2) and after (3) the stability test in methane tri-reforming reaction. Nitrogen sorption–desorption isotherms are shifted along the Y axis (for ease of comparison).

According to the XRD analysis, the fresh  $\text{Ce}_{0.2}\text{Ni}_{0.8}\text{O}_{1.2}/\text{Al}_2\text{O}_3$  catalyst includes a support phase, which is a mixture of two modifications ( $\gamma$ - and  $\delta$ -) of aluminum oxide, as well as trace amounts of the cerium (IV) oxide based phase characterized by a cubic modification of the fluorite structure and a nickel (II) oxide phase. As a result of the treatment in situ in He at 800 °C before the reaction, the  $(\gamma+\delta)\text{-Al}_2\text{O}_3$  and  $\text{CeO}_2$  phases are observed. Compared to the fresh sample, the formal parameter of aluminum oxide increases ( $7.914 \rightarrow 7.947 \text{ \AA}$ ), which indicates the formation of a Ni-Al-O solid solution based on the spinel structure of aluminum oxide. After the stability test, in addition to the  $(\gamma+\delta)\text{-Al}_2\text{O}_3$  and  $\text{CeO}_2$  phases in the catalyst, phases of nickel oxide and metallic nickel are observed (Table 2) with approximately the same value of the coherent scattering region (20 and 17 nm respectively).

For a more detailed study of the structural properties, the samples were examined by TEM (Fig. 5).

The fresh sample includes  $\gamma$ - and  $\delta\text{-Al}_2\text{O}_3$  support phases, on the surface of the crystallites of which various forms of stabilization of cerium and nickel cations are found [25]. In particular, cerium and nickel are found both as single atoms doping the support and as small crystallites (1.5–4 nm), consisting of  $\text{CeO}_2$ , NiO with a disordered structure and a highly defective substitutional solid solution  $\text{Ce}_x\text{Ni}_{1-x}\text{O}_y$  on the surface of the support. In the sample

before the stability test (after the treatment in situ in He at 800 °C), nickel and cerium are predominantly distributed evenly over the surface of the alumina. Nickel cations are stabilized in the form of dispersed particles (2–4 nm) of the Ni-Al-O solid solution and larger particles (10–15 nm) of the NiO. After the stability test (100 h on stream at 800 °C), the sample contains mainly particles of metallic nickel with a size of 10–15 nm, as well as their agglomerates with a size of up to 100 nm (Fig. 5c–e). Some nickel is present as NiO particles which are hollow inside (Fig. 5d). Part of Ni particles is encapsulated with carbon due to the tubular growth of carbon deposits (Fig. 5e). Large (100–200 nm) deposits of multi-layer carbon were also observed. These carbon deposits, as well as C-tubes, contain Ni nanoparticles, thus their growth promotes the detachment of Ni particles from the support. Cerium is stabilized in the form of highly dispersed particles and clusters (Fig. 5c), with part of the cerium still remaining in ionic form in the  $\text{Al}_2\text{O}_3$  support structure, as seen in HAADF-STEM images.

Thermal analysis of the spent catalyst showed that the amount of carbon deposits formed during 100 h of reaction was ~7 wt.% (Fig. 6), which corresponds to the carbon accumulation rate of 0.7 mgC/(g<sub>cat</sub>·h). Carbonaceous deposits are heterogeneous, as evidenced by two minima in the DTG curve at 515 and 800 °C. Based on TEM data, the first type

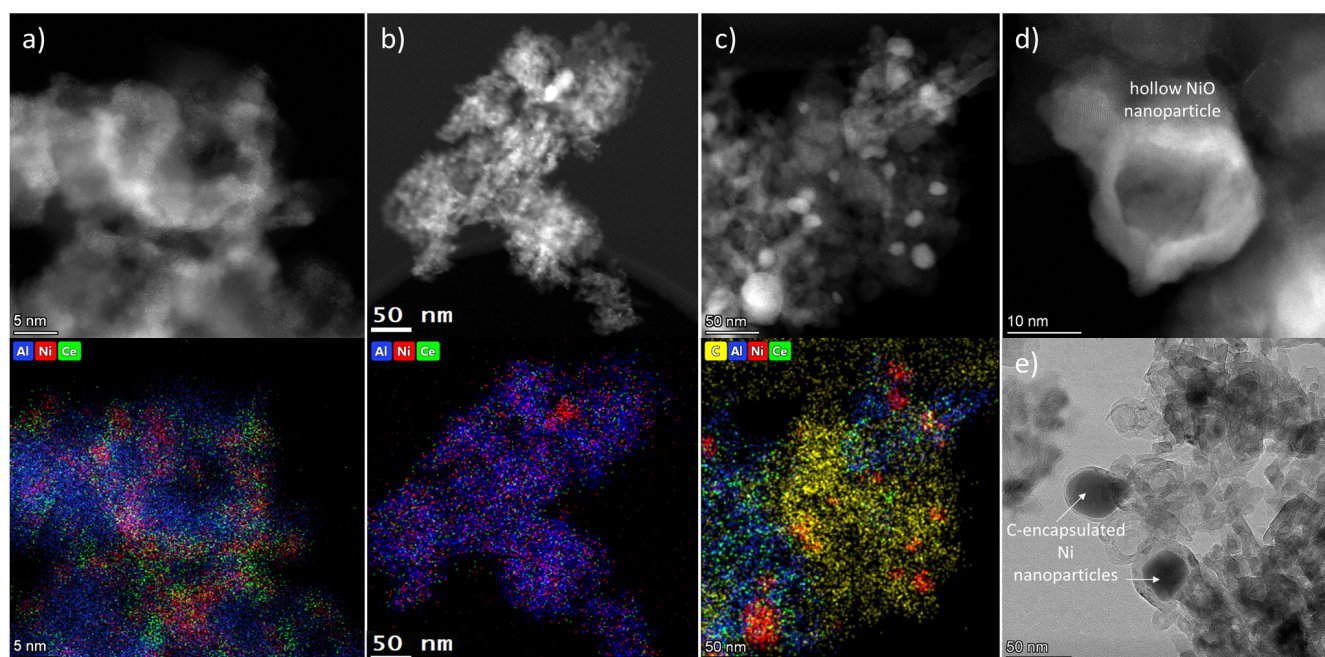


**Fig. 5.** HAADF-STEM images of the regions of the  $\text{Ce}_{0.2}\text{Ni}_{0.8}\text{O}_{1.2}/\text{Al}_2\text{O}_3$  catalyst after calcination at 500 °C (a), before (b) and after (c) stability test and the corresponding EDX mapping images (d–g) showing the distribution of aluminum (green), nickel (red), cerium (blue) and carbon (yellow) in the selected regions; HAADF-STEM (d) and TEM (e) images showing hollow NiO and C-encapsulated Ni nanoparticles in the  $\text{Ce}_{0.2}\text{Ni}_{0.8}\text{O}_{1.2}/\text{Al}_2\text{O}_3$  catalyst after stability test.

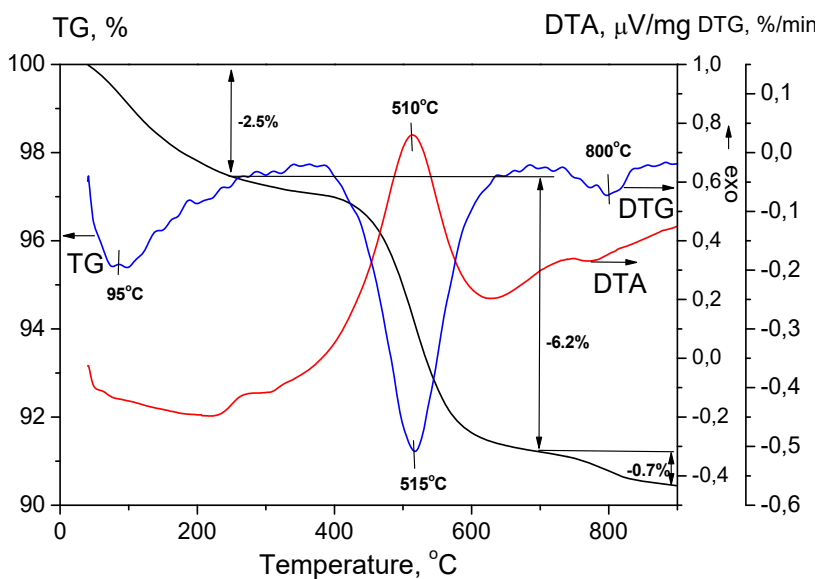


Fig. 6. Thermal analysis of the  $\text{Ce}_{0.2}\text{Ni}_{0.8}\text{O}_{1.2}/\text{Al}_2\text{O}_3$  catalyst after stability test.

of carbon deposits is carbon closely associated with metallic Ni, which catalyzes its burnout. The second type is multi-walled carbon filaments, which have a high degree of condensation, are weakly bound to the catalyst and burn out at a higher temperature.

### 3.3. Correlations between catalytic properties and catalyst structure

To identify correlations, a comparative analysis of the catalytic properties of the catalyst and its physicochemical characteristics was carried out.

In the process of tri-reforming methane in the presence of a  $\text{Ce}_{0.2}\text{Ni}_{0.8}\text{O}_{1.2}/\text{Al}_2\text{O}_3$  catalyst, no decrease in process performance was observed. On the contrary, with increasing reaction duration, the conversion of reagents and the yield of products increased slightly, which can be due to the gradual generation of active NiO sites from the slow reduction of  $\text{Ni}^{2+}$  in the Ni-Al-O solid solution during the reaction. This Ni-Al-O joint phase was formed prior to the reaction by treatment in helium at 800 °C, as shown by X-ray diffraction and TEM analysis. It was demonstrated [29,30] that the difficult reduction of  $\text{Ni}^{2+}$  in Ni-Mg-O solid solution generates nickel nanoparticles with a size smaller than the minimum Ni size required for coke formation and prevents Ni nanoparticles from sintering.

The  $\text{CO}_2$  conversion (~50%) was lower than the  $\text{CH}_4$  conversion (~80%) during all time of operation. A similar situation was observed during the tri-reforming of feedstock with a  $\text{CH}_4/\text{O}_2/\text{H}_2\text{O}/\text{CO}_2$  ratio of 1:0.1:0.0125:0.5, where at 700 °C within 50 h the

conversion of  $\text{CH}_4$  and  $\text{CO}_2$  was ~86% and ~28%, respectively, in the presence of 5 wt.% Ni/ZrO<sub>2</sub> [31]. At the composition of feedstock with a  $\text{CH}_4/\text{O}_2/\text{H}_2\text{O}/\text{CO}_2$  ratio of 1:0.1:0.9:0.67, at 800 °C and 1.4 bar the  $\text{CH}_4$  conversion was ~90% while the  $\text{CO}_2$  conversion was also lower and fluctuated between 35 and 50% during 300 hours-on-stream [32]. An increase in the  $\text{CO}_2$  conversion can be facilitated by the introduction of Mg or La oxides into the catalyst composition [33–35]. The coal mine methane tri-reforming reaction used three oxygen-containing reagents ( $\text{O}_2$ ,  $\text{H}_2\text{O}$  and  $\text{CO}_2$ ) with a  $\text{CH}_4/\text{O}_2/\text{H}_2\text{O}/\text{CO}_2$  molar ratio of 1/0.24/0.32/0.36. There is competition between these molecules for the active sites of the catalyst. So, at a high mole fraction of oxygen and/or water, the  $\text{CO}_2$  conversion decreases. In addition, the high concentration of water in the system favors the steam reforming reaction of CO, which reduces the conversion of  $\text{CO}_2$ . It is believed [36] that oxygen, as the most reactive component, is completely consumed in the reaction of total or partial oxidation of methane, mainly in the upper layer of the catalyst. Thus, after stability testing, the  $\text{Ce}_{0.2}\text{Ni}_{0.8}\text{O}_{1.2}/\text{Al}_2\text{O}_3$  catalyst contains NiO particles along with  $\text{Ni}^0$  particles.

As a result of the long-term operation of the  $\text{Ce}_{0.2}\text{Ni}_{0.8}\text{O}_{1.2}/\text{Al}_2\text{O}_3$  catalyst, some sintering of the Ni-containing phase was observed, which, however, did not lead to a deterioration in its activity. It is typical for high-loading catalysts in the high-temperature reforming process. In particular, for 5 wt.% Ni/HAP (hydroxyapatite support  $\text{Ca}_{10}(\text{PO}_4)_6(\text{OH})_2$ ) catalyst the fresh sample exhibited  $\text{Ni}^0$  particles ranging from 10 to 90 nm, while after 50 h on stream in



tri-reforming reaction, larger nickel particles up to 170–180 nm appeared [32]. It is supposed [32] that this thermal sintering quickly happened in the first minutes of the reaction, and did not further evolve, which allowed keeping the catalyst stable for the rest of reaction time.

Despite some excess of the oxidizing agent (molar ratio O/C = 1.1), the formation of a by-product – carbon deposits – was observed in the process without influence on the catalytic properties with time on stream. The rate of their accumulation was low 0.7 mgC/(g<sub>cat</sub>·h) and comparable to known literature values [32,37]. Further optimization of the catalyst composition or its preparation mode is necessary to increase CO<sub>2</sub> conversion and reduce the rate of formation of carbon deposits.

#### 4. Conclusions

A long-term test of the tri-reforming process of the methane-air mixture recovered by mine drainage systems of the Rospadskaya mine was carried out. The catalyst testing was carried out in a flow quartz reactor at atmospheric pressure, contact time 0.15 s, flow rate 200 ml/min, at 800 °C for 100 hours. The methane-air mixture containing ~35 vol.% CH<sub>4</sub>, ~9 vol.% O<sub>2</sub>, ~11 vol.% CO<sub>2</sub>, ~13 vol.% H<sub>2</sub>O and traces of C<sub>2</sub>H<sub>6</sub> and C<sub>3</sub>H<sub>8</sub>, was successfully converted into syngas containing ~42 vol.% H<sub>2</sub> and ~25 vol.% CO. After 100 h of the process, the hydrogen yield was 85% at methane conversion of 80%. The Ce<sub>0.2</sub>Ni<sub>0.8</sub>O<sub>1.2</sub>/Al<sub>2</sub>O<sub>3</sub> material, prepared by the citrate sol-gel method and containing ~10 wt.% Ni and 6 wt.% Ce, was used as a catalyst for the tri-reforming process. The changes occurring in the catalyst under reaction conditions were traced using the methods of low-temperature nitrogen adsorption, powder X-ray diffraction, electron microscopy and thermal analysis. It was found that after 100 h of the reaction the textural characteristics of the catalyst moderately decrease and the average particle size of the Ni-containing phase increases. It was revealed that during the reaction, carbon deposits of various types are formed with a carbon accumulation rate of 0.7 mgC/(g<sub>cat</sub>·h). The observed changes in the textural and structural properties of the catalyst are not critical, since they do not affect the efficiency of the process, which remained stable over 100 h of reaction. The conducted studies indicate the promise of coal mine methane conversion technology using the tri-reforming method for reducing methane emissions into the atmosphere, preserving this valuable fossil resource, and increasing the safety of underground coal mining.

#### Funding

This research was funded by the Russian Science Foundation under Project No. 22-13-20040, <https://rscf.ru/project/22-13-20040/> and from the Region – the Kemerovo Region – Kuzbass (in part of synthesis and catalytic activity investigation), project number FWUR-2024-0033 (in part of electron microscopy study and analysis of correlations between catalyst structure and catalytic properties).

#### Acknowledgements

The TEM studies were carried out using facilities of the shared research center “National center of investigation of catalysts” at the Boreskov Institute of Catalysis. The authors also acknowledge the resource center “VTAN” (Novosibirsk State University) for granting access to TEM equipment. Authors gratitude to the Ministry of Science and Education of the Russian Federation.

#### References

- [1]. Coal 2023. Analysis and forecast to 2026, INTERNATIONAL ENERGY AGENCY [https://iea.blob.core.windows.net/assets/a72a7ffa-c5f2-4ed8-a2bf-eb035931d95c/Coal\\_2023.pdf](https://iea.blob.core.windows.net/assets/a72a7ffa-c5f2-4ed8-a2bf-eb035931d95c/Coal_2023.pdf)
- [2]. Number of operational coal power plants worldwide from 2021 to 2024. <https://www.statista.com/statistics/1448736/number-of-operational-coal-power-plants-worldwide/#:~:text=Global%20active%20coal%2Dfired%20power%20stations%202021%2D2024&text=There%20are%202%2C422%20operational%20coal,countries%20continue%20their%20phase%2Dout>
- [3]. H. Ritchie, P. Rosado, Electricity Mix, (2024). <https://ourworldindata.org/electricity-mix>
- [4]. R.V. Ramani, M.A. Evans, Underground mining: in coal mining. Encyclopedia Britannica. <https://www.britannica.com/technology/coal-mining>
- [5]. Global coal miners and the urgency of a just transition. Global Energy Monitor. [https://globalenergymonitor.org/wp-content/uploads/2023/09/GEM\\_Coal\\_Mine\\_Employment\\_2023.pdf](https://globalenergymonitor.org/wp-content/uploads/2023/09/GEM_Coal_Mine_Employment_2023.pdf)
- [6]. Top 10 most dangerous jobs in the United States in 2024. Industrial Safety and Hygiene News. [https://www.ishn.com/articles/114334-top-10-most-dangerous-jobs-in-the-united-states-in-2024#:~:text=The%20top%2010%20most%20dangerous%20jobs%20in%20the%20U.S.%20in,r-ecycling%20collection%3B%208\)%20iron%20and](https://www.ishn.com/articles/114334-top-10-most-dangerous-jobs-in-the-united-states-in-2024#:~:text=The%20top%2010%20most%20dangerous%20jobs%20in%20the%20U.S.%20in,r-ecycling%20collection%3B%208)%20iron%20and)

- [7]. I.I. Mokhnachuk, T.E. Piktushanskaya, M.S. Bryleva, K.V. Betts, *Russ. J. Occup. Heal. Ind. Ecol.* 63 (2023) 88–93 (in Russ.). DOI:10.31089/1026-9428-2023-63-2-88-93
- [8]. Tabas coal mine explosion. [https://en.wikipedia.org/wiki/2024\\_Tabas\\_coal\\_mine\\_explosion](https://en.wikipedia.org/wiki/2024_Tabas_coal_mine_explosion)
- [9]. D. Strapoć, F.W. Picardal, C. Turich, et al., *Appl. Environ. Microbiol.* 74 (2008) 2424–2432. DOI:10.1128/AEM.02341-07
- [10]. B. Saha, A.S. Patra, A.K. Mukherjee, *J. Mol. Graph. Model.* 106 (2021) 107868. DOI:10.1016/j.jmgm.2021.107868
- [11]. United Nations Economic Commission for Europe, Best Practice Guidance for Effective Methane Drainage and Use in Coal Mines. ECE ENERGY SERIES No. 47, Second edition, 2016. [https://unece.org/fileadmin/DAM/energy/cmm/docs/BPG\\_2017.pdf](https://unece.org/fileadmin/DAM/energy/cmm/docs/BPG_2017.pdf)
- [12]. N. Kholod, M. Evans, R.C. Pilcher, et al., *J. Clean. Prod.* 256 (2020) 120489. DOI:10.1016/j.jclepro.2020.120489
- [13]. O.V. Tailakov, MIAB. *Mining Inf. Anal. Bull.* [Gornyj informacionno-analiticheskij bjulleten'] 11 (2024) 88–100. (in Russ.). DOI:10.25018/0236\_1493\_2024\_11\_0\_88
- [14]. Order of the Federal Service for Environmental, Technological and Nuclear Supervision dated December 8, 2020 No. 506 “On approval of Federal norms and regulations in the field of industrial safety “Instructions for aerological safety of coal mines”. (in Russ.). <http://publication.pravo.gov.ru/document/0001202012300105?index=1>
- [15]. Global Methane Initiative (GMI). International Coal Mine Methane Project List. <https://globalmethane.org/resources/details.aspx?resourceid=1981>
- [16]. J. Yin, S. Su, J.S. Bae, et al., *Energy Fuel.* 34 (2020) 655–664. DOI:10.1021/acs.energyfuels.9b03076
- [17]. E.V. Matus, I.Z. Ismagilov, E.S. Mikhaylova, Z.R. Ismagilov, *Eurasian Chem.-Technol. J.* 24 (2022) 69–91. DOI:10.18321/ectj1320
- [18]. X. Wang, K. Wei, S. Yan, et al., *Appl. Catal. B Environ.* 268 (2020) 118413. DOI:10.1016/j.apcatb.2019.118413
- [19]. K. Wei, X. Wang, H. Zhu, et al., *J. Power Sources* 506 (2021) 230208. DOI:10.1016/j.jpowsour.2021.230208
- [20]. H. Zhu, H. Dai, Z. Song, et al., *Int. J. Hydrogen Energy* 46 (2021) 31439–31451. DOI:10.1016/j.ijhydene.2021.07.036
- [21]. I.V. Sedov, V.S. Arutyunov, M.V. Tsvetkov, et al., *Eurasian Chem.-Technol. J.* 24 (2022) 157–163. DOI:10.18321/ectj1328
- [22]. E.V. Matus, Z.R. Ismagilov, *Eurasian Chem.-Technol. J.* 24 (2022) 203–214. DOI:10.18321/ectj1433
- [23]. E.V. Matus, M.A. Kerzhentsev, A.P. Nikitin, et al., *Eurasian Chem.-Technol. J.* 25 (2023) 103–113. DOI:10.18321/ectj1500
- [24]. E.V. Matus, M.A. Kerzhentsev, A.P. Nikitin, et al., *Eurasian Chem.-Technol. J.* 26 (2024) 3–14. DOI:10.18321/ectj1559
- [25]. E.V. Matus, E.N. Kovalenko, A.V. Kapishnikov, et al., *J. Struct. Chem.* 65 (2024) 1692–1706. DOI:10.1134/S0022476624090026
- [26]. E. Matus, O. Sukhova, M. Kerzhentsev, et al., *Catalysts* 12 (2022) 1493. DOI:10.3390/catal12121493
- [27]. A.V. Salnikov, E.V. Matus, M.A. Kerzhentsev, S.R. Khairulin, *Chem. Sustain. Dev.* 32 (2024) 384–392. DOI:10.15372/CSD2024569
- [28]. K.S.W. Sing, *Pure Appl. Chem.* 57 (1985) 603–619. DOI:10.1351/pac198557040603
- [29]. E. Ruckenstein, Y.H. Hu, *Appl. Catal. A Gen.* 133 (1995) 149–161. DOI:10.1016/0926-860X(95)00201-4
- [30]. Y.H. Hu, E. Ruckenstein, *Science* 368 (2020) 5459. DOI:10.1126/science.abb5459
- [31]. A. Pandey, P. Biswas, K.P. Kishore, A.K. Dalai, *Ind. Eng. Chem. Res.* 63 (2024) 1000–1012. DOI:10.1021/acs.iecr.3c03645
- [32]. T.S. Phan, D.P. Minh, *ChemCatChem* 16 (2024) e202400192. DOI:10.1002/cctc.202400192
- [33]. X.H. Pham, U.P.M. Ashik, J.I. Hayashi, et al., *Appl. Catal. A Gen.* 623 (2021) 118286. DOI:10.1016/j.apcata.2021.118286
- [34]. D.P. Minh, X.H. Pham, T.J. Siang, D.V.N. Vo, *Appl. Catal. A Gen.* 621 (2021) 118202. DOI:10.1016/j.apcata.2021.118202
- [35]. K. Świrk, T. Grzybek, M. Motak, *E3S Web Conf.* 14 (2017) 1–10. DOI:10.1051/e3sconf/20171402038
- [36]. D.M. Walker, S.L. Pettit, J.T. Wolan, J.N. Kuhn, *Appl. Catal. A Gen.* 445–446 (2012) 61–68. DOI:10.1016/j.apcata.2012.08.015
- [37]. K. Świrk Da Costa, J. Grams, M. Motak, et al., *J. CO<sub>2</sub> Util.* 42 (2022) 101317. DOI:10.1016/j.jcou.2020.101317